Substitution of Eqs. (2–4, 6, and 8) into (7) yields the expression for the net rate of mass flow through inlet scoop:

$$M = \frac{\pi r_2^2 p_\infty}{(2\pi RT_\infty)^{1/2}} \left\{ C_1 e^{-S^2} + C_2(\pi)^{1/2} S(1 + \text{erf}S) - C_3(\pi)^{1/2} S \left[1 + \text{erf} \frac{LS}{(L^2 + r_1^2)^{1/2}} \right] e^{-r_1^2 S^2/(L^2 + r_1^2)} - C_4 \frac{p_c}{p_\infty} \left(\frac{T_\infty}{T_c} \right)^{1/2} \right\} \quad (9)$$

where

$$C_1 = \frac{r_1^2[(L^2 + r_1^2 + r_2^2)\phi^2 - (L^2 + r_1^2)^2 + 2r_1^2 r_2^2 - r_2^4]}{2r_2^2(L^2 + r_1^2)(\phi^2 - L^2)}$$

$$C_2 = \frac{r_1^2 + r_2^2}{2r_2^2} - \frac{(r_1^2 - r_2^2)^2}{2r_2^2(\phi^2 - L^2)}$$

$$C_3 = \frac{L^3(\phi^2 - L^2 + r_1^2 - r_2^2)}{2(\phi^2 - L^2)(L^2 + r_1^2)^{3/2}}$$

$$C_4 = \frac{(L^2 + r_1^2 + r_2^2)\phi^2 - \phi^4}{2r_2^2(\phi^2 - L^2)}$$

If no inlet scoop is used, Eq. (9) reduces to the expression for the mass flow rate through a circular aperture of negligible lip thickness:

$$M_0 = [\pi r_2^2 p_\infty/(2\pi RT_\infty)^{1/2}] \; [e^{-S^2} + (\pi)^{1/2} S(1 + \text{erf}S)] \quad (10)$$

The dimensionless mass flow rate through inlet scoop is defined as the ratio of M to M_0. For any given value of S and $(p_c/p_\infty)/(T_\infty/T_c)^{1/2}$, the mass flow rates can be plotted as functions of scoop geometry (i.e., L/r_2 and r_1/r_2, e.g., see Fig. 1). From these curves it can be seen that, for any given scoop length ratio (L/r_2), there exists an optimum scoop geometry through which the mass flow rate reaches a maximum value.

It is coincident with the author's intuitive prediction that the maximum mass flow rate increases as the size of the scoop and the freestream velocity ratio increase. However, when S approaches infinity and $r_1^2 = r_2^2 + (2r_2^2 + 2L^2)^{1/2}$, then M/M_0 attains a maximum value

$$\lim_{S \to \infty} \left(\frac{M_{\max}}{M_0} \right) = \frac{2L^2 + 3r_2^2 + 2(2r_2^2 + 2L^2)^{1/2}}{L^2 + 2r_2^2 + 2(2r_2^2 + 2L^2)^{1/2}}$$

From this one can see clearly that the gain of mass flow rate with the aid of a big scoop is limited by a factor of two.

In the design of inlet scoops, for any given value of L/r_2 a family of curves for M/M_0 vs r_1/r_2 may be plotted. For $S > 1$, the maximum mass flow rates occur almost at the same value of r_1/r_2, and, for $S > 2$, all curves are very close to one another. As an example, when $L/r_2 = 2$, the maximum mass flow rate can be maintained for a very wide range of freestream velocity when $r_1/r_2 = 1.98$, and, for $S > 2$, the mass flow rate through this inlet scoop can be represented by a simple formula:

$$M = 1.392 \; \rho_\infty U_\infty A_2$$

Numerical solutions for the dimensionless mass flow rate through optimum inlet scoops are obtained and plotted in Fig. 2, which is useful for the design of optimum inlet scoops at various lengths.

A similar problem concerning the free-molecule flow through a diverging duct for $S = 0$ was treated by Davis et al.,[4] who obtained some exact numerical solutions by using the Monte Carlo method. In this note the problem is treated analytically based on two important assumptions: 1) the mass flux incident on the wall is uniform, and 2) the mass flux passing directly from A_1 to A_2 without striking the wall is equal to the mass flux passing the midpoint of A_2. When $S = \infty$, these two assumptions represent the true case, and the result obtained here gives the exact solution of the problem. However, when $S = 0$, the result obtained here does not agree very well with Davis' solution, because of the two forementioned assumptions. It is believed that, if S is not very small, say $S > 1$, the result obtained here will be quite accurate for optimum geometries.

References

[1] Eckert, E. R. G., "Similarities between energy transport in rarefied gases and by thermal radiation," *Modern Developments in Heat Transfer* (Academic Press, New York, 1962), pp. 159–180.

[2] Sparrow, E. M., Jonsson, V. K., and Lundgren, T. S., "Free-molecule tube flow and adiabatic wall temperatures," AMSE-AIChE Heat Transfer Conference, Houston, Texas (August 5–8, 1962), Paper 62-HT-35.

[3] Eckert, E. R. G. and Drake, R. M., *Heat and Mass Transfer* (McGraw-Hill Book Co. Inc., New York, 1959), p. 398.

[4] Davis, D. H., Levenson, L. L., and Milleron, N., "Theoretical and experimental studies of molecular flow through short ducts," *Rarefied Gas Dynamics*, edited by L. Talbot (Academic Press, New York, 1961), pp. 99–115.

Impact Force and Crater Surface Area

R. F. Rolsten* and H. H. Hunt†

General Dynamics/Astronautics, San Diego, Calif.

Nylon, glass, and aluminum projectiles impacting on aluminum at velocities of 3.78 to 5.43 × 10^5 cm/sec produce hemispherical craters. The impact damage can be related to the tensile strength by using equations for uniformly accelerated rectilinear motion when the measured crater dimensions are corrected for relaxation after the pressure release. Steel projectiles do not conform to this impact model.

Nomenclature

P = pressure applied to the target, dynes/cm^2
A = surface area of crater, cm^2
F = force applied to the target, dynes
W = work
m = mass of projectile, g
v = velocity of projectile, cm/sec
d = distance (penetration depth or radius of the hemispherical crater) through which the force is applied, cm
d' = projectile diameter, cm
a = acceleration (or deceleration), cm/sec^2
ρ_P = projectile density, g/cm^3
ρ_T = target density, g/cm^3
C_T = speed of sound in target, cm/sec

Introduction

BEHAVIOR of materials subjected to high velocity impact (impulsive loading) has led to concepts that do not follow conventional loading problems. These concepts depend upon the elements of time and motion. Thus, when a material is subjected to an impulsive load (element of time), the motion may attain a value that is critical with regard to the initiation of a specific mode of behavior.

The effect of high pressure on the bulk physical and mechanical properties may be very pronounced under impulsive loading since pressures of several hundred thousand pounds per square inch are attained frequently. Peak pressures are attained in about 10^{-6} to 10^{-7} sec. These high pressure

Received by IAS November 20, 1962; revision received June 4, 1963.

* Associate Professor at California Western University.

† Chemist.

effects on the mechanical properties may be generalized as follows[1, 2]:

1) The tension and compression strengths of most metallic elements are increased at very high pressures.

2) The rigidity of metals generally increases linearly with pressure.

3) Young's modulus increases, with increasing pressure, by an amount intermediate between the increase of rigidity and incompressibility.

4) The ability to undergo large amounts of plastic deformation increases with increasing pressure.

In any real impact, elastic and plastic effects in both the target and projectile must be taken into consideration. The physical nature of inelastic processes are not known clearly and precise theoretical treatments have not been completely satisfactory. At very high stress levels, the body may undergo permanent deformation and/or lose its rigidity and behave as a fluid. Failure by plastic flow and fracture can influence the disturbance. Mechanical properties of the body being loaded may be time dependent, i.e., 1) have a time delay for initiation of plastic flow[3–5]; 2) show an increase in yield and ultimate strength with the rate of delivery of the load[6, 7]; and 3) be influenced by the stress within the body.[8]

Internal friction may lead to an attenuation of the intensity of the disturbance as a result of energy absorption. Thus, the disturbance will tend to lengthen since its momentum must be conserved even though its energy is dissipated.[9, 10]

Experimental

Projectiles of steel, aluminum, glass, and nylon were accelerated with a light gas and powder gun in a vacuum. Spherical projectiles with impact masses in the range between 0.075 to 0.800 g were accelerated to velocities from 3.78×10^5 to 5.43×10^5 cm/sec (15,220 to 17,800 fps). The impact masses of projectiles accelerated in vacuum were assumed to be identical with the accelerated masses since aerodynamic effects were minimal. Data from the impact on thick aluminum plates (6061-T6) by projectiles of various composition (nylon, glass, aluminum, and steel) are summarized in Table 1. Nylon, glass, and aluminum projectiles were observed to form near hemispherical craters in aluminum as determined from the value of the crater radius to crater depth; this value is unity for hemispherical craters. Steel projectiles do not form hemispherical craters in aluminum under the experimental conditions. All aluminum target plates displayed typical hypervelocity petal formations around the lip of the crater. There is recoil (or rebound) of target material surrounding the crater upon relaxation of the impact pressure. This relationship amounts[11] to 20 to 25% for aluminum in the 2*S* condition. Since the crater dimensions are determined after this rebound has occurred, it was necessary to correct the crater measurements in order to test reliably the applicability of the equations for uniform rectilinear acceleration (deceleration) and to relate material properties to crater damage. Thus, the surface area over which the impact force was applied was assumed to be

Table 1 Summary of high velocity impact data

Exp. no.	Measured crater radius at target surface, cm	Crater radius / Crater depth	Impact velocity, cm/sec	Projectiles Material	Projectiles Mass, g
A	1.080	1.063	5.43×10^5	nylon	0.299
B	1.110	0.949	3.78	aluminum	0.777
C	0.572	0.866	4.64	glass	0.075
D	1.334	1.010	4.64	aluminum	0.800
E	0.572	1.022	4.39	glass	0.075
F	0.483	0.500	4.27	steel	0.120

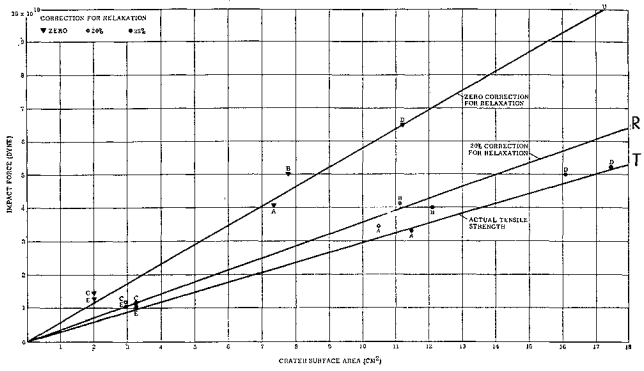

Fig. 1 Dependence of crater surface area on impact force.

a hemisphere whose radius was 20 and 25% greater than the measured radius of the crater.

Data in Table 1 are shown in Fig. 1, a plot of the impact force vs maximum surface area of the crater. Curve *U* is based on the crater depth uncorrected for relaxation; curves *R* and *T* are based on the crater depth corrected 20% for elastic rebound and the actual tensile strength of the aluminum, respectively. The slope of these two curves is $U = 5.8$ and $R = 3.6 \times 10^9$ dynes/cm^2. These values can be compared to the actual tensile strength value of 2.9×10^9 dynes/cm^2.

Discussion

Hypervelocity impact involves the action of inertia (defined by Newton's first law of motion) and the energy associated with the relative motions of mass. Momentum, the quantity of motion measured by the product of the mass and velocity, is necessary to describe the transfer of motion from one body to another. The momentum is the only quantity involved in a perfectly elastic impact. However, high velocity particles produce an inelastic collision. Thus, permanent deformation and changes will be produced in the colliding bodies with a corresponding decay or conversion of the energy of relative motion into radiation and heat. The projectile and target materials in the immediate region of the impact are melted, vaporized, compressed, and/or shattered, depending upon such parameters as the density, viscosity, physical and mechanical properties of *both* the projectile and target, particle mass, impact velocity, and angle on the target.

Rinehart[12, 13] assumed that the size and shape of a crater formed by a high velocity particle depended on the stress distribution existing in the target immediately following deceleration of the projectile. The force of the impact distributes itself within the target in accordance with the same geometry as the stresses produced by a static load. The magnitude of the shearing stress decreases with distance from the area of application of force, and it eventually becomes less than that required to cause the material to fail. There will exist a surface of failure that corresponds to a critical limiting shearing stress.

The maximum crater surface area (A) of damage to a target increases linearly with an increase in the force (F) applied by the impacting projectile as shown in Fig. 1. This linearity of F vs A is observed with projectiles of different materials and mass in the velocity range from 3.78 to 5.43×10^5 cm/sec. The slope of this line is the pressure under which the target material will just flow, or conversely, the pressure acting on the incipient crater at the instant the crater ceases to expand. Thus, crater formation will proceed only as long as the force per unit area exceeds the dynamic compressive strength of the target material.

The average calculated pressure is about 3.6 and 3.2×10^9 dynes/cm^2 when a 20 and 25%, respectively, relaxation effect

is assumed. The minimum ultimate tensile strength[14] that is acceptable for 6061 aluminum alloy in the T6 condition is 2.9×10^9 dynes/cm^2 (see Appendix). The compressive strength should be slightly higher than the tensile strength. The magnitude of this difference cannot be stated unequivocably until more accurate values of the relaxation are established experimentally. It is significant, however, that damage to aluminum via hypervelocity impact with the formation of hemispherical craters can be related to the tensile strength established by standard metallurgical techniques.

Work is performed on both the impacting particle and the target in an inelastic impact. This work is derived from the decay of energy of relative motion. As a metal target is deformed (penetrated) it will resist penetration.

Pertinent equations are summarized as follows:

$$P = F/A \tag{1}$$

$$Fd = W = 1/2mv^2 = \text{KE} \tag{2}$$

If the product of pressure and the surface area of the crater is constant throughout the process of crater formation, then the equations for uniformly accelerated (decelerated) rectilinear motion apply:

$$F = ma \tag{3}$$

$$v^2 = 2\,ad \tag{4}$$

Combining Eqs. (1, 3, and 4), it is seen that the maximum penetration in the target is given by the following expression:

$$d = mv^2/2AP \tag{5}$$

A commonly used form of the penetration equation may be derived from uniform acceleration equations if a hemispherical crater is formed. This equation takes the form

$$d/d' = \text{const}(\rho_P/\rho_T)^{1/3}(v_P/C_T)^{2/3} \tag{6}$$

where the penetration depends on the one-third power of the density ratio and the two-thirds power of the velocity ratio.

The impact of a steel projectile on an aluminum target produces a cavity whose depth approximately is equal to its diameter. Impact velocity was 4.2×10^5 cm/sec. This formation of nonhemispherical craters, impact of steel on aluminum, leads to data that do not correlate with the damage model proposed. One possible explanation for this apparent anomalous behavior may be that the steel projectile provides more resistance to flow (less viscous) than projectiles of nylon, glass, and aluminum under the conditions that prevail under impact.

Appendix

Four tensile specimens were fabricated from 6061-T6 aluminum plate used as targets in this series of tests. The experimental ultimate tensile strengths were as follows:

1) Transverse, 2.8216×10^9 dynes/cm^2.
2) Transverse, 3.1265×10^9 dynes/cm^2.
3) Longitudinal, 3.0605×10^9 dynes cm^2.
4) Longitudinal, 2.8802×10^9 dynes/cm^2.

References

[1] Bridgman, P. W., *The Physics of High Pressure* (G. Bell and Sons, Ltd., London, 1949), Chap. XIII.

[2] Bridgman, P. W., *Studies in Large Plastic Flow and Fracture* (McGraw-Hill Book Co. Inc., New York, 1952), Part I.

[3] Clark, D. S. and Wood, D. S., "The time delay for initiation of plastic deformation at rapidly applied constant stress," Am. Soc. Testing Mater. Proc. **49**, 717–735 (1949).

[4] Wood, D. S. and Clark, D. S., "The influence of temperature upon the time delay for yielding in annealed mild steel," Trans. Am. Soc. Metals **43**, 571–586 (1951).

[5] Kramer, I. R. and Maddin, R., "Delay time for the initiation of slip in metal single crystals," J. Metals **4**, 197–203 (1952).

[6] Clark, D. S. and Wood, D. S., "The tensile impact properties of some metals and alloys," Trans. Am. Soc. Metals **42**, 45–74 (1950).

[7] Ginns, D. W., "The mechanical properties of some metals and alloys broken at ultra-high speeds," J. Inst. Metals **61**, 61–78 (1937).

[8] Bridgman, P. W., "Effects of high hydrostatic pressure on the plastic properties of metals," Rev. Mod. Phys. **17**, 3–14 (1945).

[9] Kolsky, H. and Shearman, A. C., "Investigation of fractures produced by transient stress waves," Research **2**, 384–389 (1949).

[10] Rinehart, J. S., "Discussion of paper by D. S. Wood: 'On longitudinal plane waves of elastic-plastic strain in solids,' " J. Appl. Mech. **20**, 307–308 (1953).

[11] Gehring, J. W., Jr., "Observations of the phenomena of hypervelocity impact," Fourth Hypervelocity Impact Symposium, APGC-TR-60-39 (II), Paper 29 (September 1960).

[12] Rinehart, J. S., "Some observations on high-speed impact," Popular Astron. **58**, 458–464 (1950).

[13] Rinehart, J. S. and Pearson, J., *Behavior of Metals Under Impulsive Loads* (The American Society for Metals, Cleveland, Ohio, 1954), Chap. XII.

[14] *Strength of Metal Aircraft Elements*, Military Handbook-5 (March 1959), Chap. III.

Triangular Plate Elements in the Matrix Force Method of Structural Analysis

J. S. Przemieniecki*

Air Force Institute of Technology, Wright-Patterson Air Force Base, Ohio

The flexibility properties for the triangular plate element are derived for a set of three independent force systems acting along the three sides of the triangle. These systems lead to very simple patterns for the self-equilibrating (redundant) force systems which may be used in the matrix force method of analysis of structures with triangular plates. The flexibility and relative thermal displacement matrices derived for these force systems can be included in the subroutine library of flexibility properties in any of the computer programs for the analysis of complex structures.

Introduction

THE use of triangular plates as basic elements in matrix structural analysis is very attractive since such elements can be employed in the idealization of nonorthogonal panels. The triangular plate elements so far have been used mainly in the displacement method of analysis[1] in which the element forces on the triangular plates are related to the corresponding displacements through the stiffness matrices determined on the assumption of linearly varying displacements. This assumption leads to a compatible constant stress field that also satisfies the stress equilibrium equations within the triangle. Since the stresses vary from element to element there is, in general, a discontinuity in stress distribution across the boundaries of adjacent elements violating the boundary equilibrium. The satisfaction of overall equilibrium of the complete stress field is then achieved through the equilibrium of equivalent element forces at common joints.

The concept of constant stress field in triangular plates also can be applied to the matrix force method of analysis.

Received by IAS December 10, 1962; revision received June 3, 1963.

* Associate Professor and Acting Head, Department of Mechanics. Associate Fellow Member AIAA.